Article

Polychromatic Selective Population Inversion for TROSY Experiments with Large Proteins

Krystyna Bromek, Donghan Lee, Richard Hauhart, Malgorzata Krych-Goldberg, John P. Atkinson, Paul N. Barlow, and Konstantin Pervushin

J. Am. Chem. Soc., **2005**, 127 (1), 405-411• DOI: 10.1021/ja0462326 • Publication Date (Web): 04 December 2004

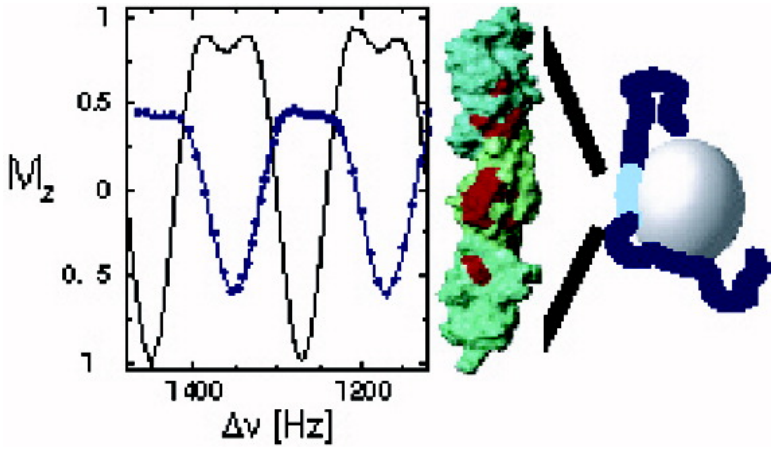

More About This Article

Additional resources and features associated with this article are available within the HTML version:

- Supporting Information
- Links to the 2 articles that cite this article, as of the time of this article download
- Access to high resolution figures
- Links to articles and content related to this article
- Copyright permission to reproduce figures and/or text from this article

View the Full Text HTML

J|A|C|S
ARTICLES
Published on Web 12/04/2004

Polychromatic Selective Population Inversion for TROSY Experiments with Large Proteins

Krystyna Bromek,[†] Donghan Lee,[‡] Richard Hauhart,[§] Malgorzata Krych-Goldberg,[§] John P. Atkinson,[§] Paul N. Barlow,[†] and Konstantin Pervushin*[,‡]

Contribution from the Laboratory of Physical Chemistry, Swiss Federal Institute of Technology, ETH-Hönggerberg, CH-8093 Zürich, Switzerland, Schools of Biological Sciences and Chemistry, University of Edinburgh, Joseph Black Building, Edinburgh, EH9 3JJ United Kingdom, and Division of Rheumatology, School of Medicine, Washington University, St. Louis, Missouri 63110

Received June 25, 2004; E-mail: kope@phys.chem.ethz.ch

Abstract: This paper presents polychromatic selective polarization inversion (PC−SPI) as an alternative to the polarization transfer methods recently developed for the application of NMR to large biological molecules. Theoretical and numerical considerations indicate that PC−SPI has the potential for more efficient polarization transfer under conditions of rapid transverse relaxation compared to *J* coupling- and cross-correlated relaxation-based transfers. The main advantage offered by the method presented here is the maintenance of near-optimal trajectories of inversion of the individual components of the spin magnetization while using broadband optimized pulses. A 2D experiment was implemented combining PC−SPI with TROSY-based chemical shift correlation. The experiment was applied to detect $^{15}N-^{1}H$ chemical shift correlation spectra of a 200 kDa complex consisting of an 80% ^{2}H- and uniformly ^{15}N,^{13}C-labeled 22 kDa portion of complement receptor type 1 and unlabeled C3b of complement (180 kDa).

Introduction

The major problems associated with applications of solution NMR techniques to large proteins are fast transverse relaxation of the spins of interest and the complexity of the NMR spectra, both of which increase with increasing molecular size.[1−6] The use of transverse relaxation optimized spectroscopy (TROSY)[7] together with uniform deuteration[8−11] reduces the transverse relaxation rates of ^{1}HN, ^{15}N, and ^{13}Caromatic spins. TROSY-based triple resonance 3D and 4D NMR experiments have been developed[12−15] enabling successful assignment of the backbone resonances in large biomolecules. When subjected to this approach, many large systems have yielded spectra of manageable complexity. Examples include multimeric proteins with internal symmetry or selectively isotopically labeled proteins in supramolecular complexes.[5,6] Even if the detailed 3D structure is not obtainable, TROSY-type direct correlation experiments are useful in chemical shift mapping of intermolecular contacts in large complexes. For example, using TROSY, the contact sites for themannose-binding type-1 pilus subunit FimH were identified on the surface of the NMR-derived structure of the two-domain periplasmic chaperone FimC from *Esherichia coli* by ^{15}N and ^{1}H NMR chemical shift mapping.[16] NOE steady-state cross-relaxation combined with TROSY allowed identification of the binding surface of protein A for the Fc portion of immunoglobulin G.[17] The interaction between the lectin chaperone calreticulin and the thiol-disulfide oxidoreductase was mapped by TROSY,[18] and further analysis provided information on the thermodynamics and kinetics of complex formation. In very large complexes, CRINEPT and CRIPT techniques in combination with TROSY have resulted in successful interpretation of 2D NMR spectra of GroES in 472 kDa GroES−SR1 and 900 kDa GroES−GroEL complexes.[19,20]

[†] Swiss Federal Institute of Technology.
[‡] University of Edinburgh.
[§] Washington University.

(1) Wagner, G. *J. Biomol. NMR* **1993**, *3*, 375−385.
(2) Kay, L. E.; Gardner, K. H. *Curr. Opin. Struct. Biol.* **1997**, *7*, 722−731.
(3) Clore, G. M.; Gronenborn, A. M. *Nat. Struct. Biol.* **1997**, *4 Suppl.*, 849−853.
(4) Clore, G. M.; Gronenborn, A. M. *Curr. Opin. Chem. Biol.* **1998**, *2*, 564−70.
(5) Pervushin, K. V. *Q. Rev. Biophys.* **2000**, *33*, 161−197.
(6) Wider, G.; Wuthrich, K. *Curr. Opin. Struc. Biol.* **1999**, *9*, 594−601.
(7) Pervushin, K.; Riek, R.; Wider, G.; Wuthrich, K. *Proc. Natl. Acad. Sci. U.S.A.* **1997**, *94*, 12366−12371.
(8) LeMaster, D. M. *Methods Enzymol.* **1989**, *177*, 23−43.
(9) LeMaster, D. M. *Annu. Rev. Biophys. Biophys. Chem.* **1990**, *19*, 243−266.
(10) LeMaster, D. M. *Q. Rev. Biophys.* **1990**, *23*, 133−174.
(11) Venters, R. A.; Farmer, B. T.; Fierke, C. A.; Spicer, L. D. *J. Mol. Biol.* **1996**, *264*, 1101−1116.
(12) Salzmann, M.; Wider, G.; Pervushin, K.; Senn, H.; Wuthrich, K. *J. Am. Chem. Soc.* **1999**, *121*, 844−848.
(13) Salzmann, M.; Pervushin, K.; Wider, G.; Senn, H.; Wuthrich, K. *Proc. Natl. Acad. Sci. U.S.A.* **1998**, *95*, 13585−13590.
(14) Yang, D. W.; Kay, L. E. *J. Am. Chem. Soc.* **1999**, *121*, 2571−2575.
(15) Konrat, R.; Yang, D. W.; Kay, L. E. *J. Biomol. NMR* **1999**, *15*, 309−313.
(16) Pellecchia, M.; Sebbel, P.; Hermanns, U.; Wuthrich, K.; Glockshuber, R. *Nat. Struct. Biol.* **1999**, *6*, 336−339.
(17) Takahashi, H.; Nakanishi, T.; Kami, K.; Arata, Y.; Shimada, I. *Nat. Struct. Biol.* **2000**, *7*, 220−223.
(18) Frickel, E. M.; Riek, R.; Jelesarov, I.; Helenius, A.; Wuthrich, K.; Ellgaard, L. *Proc. Natl. Acad. Sci. U.S.A.* **2002**, *99*, 1954−1959.
(19) Riek, R.; Fiaux, J.; Bertelsen, E. B.; Horwich, A. L.; Wuthrich, K. *J. Am. Chem. Soc.* **2002**, *124*, 12144−12153.
(20) Fiaux, J.; Bertelsen, E. B.; Horwich, A. L.; Wuthrich, K. *Nature* **2002**, *418*, 207−211.

10.1021/ja0462326 CCC: $30.25

Critical to all these studies is polarization transfer between the most sensitive spins, such as protons, and heteronuclear spins, such as carbon-13 or nitrogen-15.[21] When relaxation rates of the corresponding coherencies become comparable to the spin−spin couplings, the efficiency of polarization transfer is considerably reduced, leading to poor sensitivity and significantly increased measurement time. Currently, the most widely employed techniques for achieving polarization transfer are based on the evolution of the density operator under the effects of scalar or dipolar couplings,[22−24] cross-correlated relaxation,[25] or both.[26,27] Alternatively, polarization transfer between scalar coupled spins can be achieved by a selective inversion, or saturation, of one of the spin transitions. This is known as selective population inversion (SPI)[28−34] or transfer (SPT).[35,36] Such selective inversions have been employed in a range of applications including selective measurements of relaxation rates.[37,38] Glaser et al.[27,39] established the boundary of polarization transfer in a two-spin $^1/_2$ system subjected to relaxation, and this group proposed the use of pulse sequence elements to drive the density operator along a theoretically optimal (geodesic) pathway. Unfortunately, this solution applies only to the case where the resonance frequencies of a single spin pair (*I* and *S*) are known. Although experiments have been proposed that implement selective pulse-based Hadamard-type broadband chemical shift correlations,[40−44] theoretically optimal broadband excitation,[45] and coherence transfer,[46] none have so far been applied to large proteins.

In the present communication, we show that optimization of pulse sequences using the favorable relaxation properties of the rf-propagated density operator under SPI can be employed to construct a 2D broadband chemical shift correlation experiment. We demonstrate that this method features a significantly higher efficiency of polarization transfer, under the influence of rapid relaxation, compared to routinely used techniques. This would be expected to benefit NMR studies of large proteins and protein complexes in solution. The technique has therefore been applied to chemical shift mapping of the 198 kDa complex formed between an 80%-^{2}H,^{15}N,^{13}C-labeled fragment of complement receptor type 1 (the immune adherence receptor) encompassing the functional site 2 (CR1, site 2) and the unlabeled opsonising complement protein C3b (CR1/C3b complex).

Methods

Selective Population Inversion (SPI) in the Presence of Relaxation. In two-spin $^1/_2$ *IS* system representing, for example, a ^{1}H−^{15}N moiety (denoted *I* and *S*, respectively), selective inversion of one of the two ^{1}H transitions results in the creation of two-spin order:

$$I_z = {}^1/_2\,(I_z^{\alpha} + I_z^{\beta}) \rightarrow {}^1/_2\,(I_z^{\alpha} - I_z^{\beta}) = 2I_zS_z$$

This is maximized by a complete inversion of one of the single-transition operators, I_z^{α} or I_z^{β}, attained by the use of a selective pulse. This is also true for the conventional INEPT scheme, which exploits the evolution of the density operator under *J* scalar coupling.[22] The main advantage of SPI over INEPT, however, resides in the favorable relaxation properties of the density operators generated along the spin trajectory in the polarization transfer. To compare SPI and INEPT in terms of the efficiency of the polarization transfer each can achieve under the influence of relaxation, we used an adiabatic approximation suitable for the *IS* spin system in a large molecule.

We restricted relaxation effects in the *IS* spin system to two major interactions, the dipole−dipole and chemical shift anisotropy (CSA) interaction. To simplify the analysis, we introduced several assumptions. (i) Longitudinal relaxation rates are negligibly small when compared to the transverse relaxation rates. (ii) The coherences described by $I_{x,y}^{\alpha}$ and $I_{x,y}^{\beta}$ operators decay monoexponentially with the characteristic relaxation rates:

$$1/T_2^{\alpha} = 4J(0)(p^2 - 2\,C_{kl}\,p\,\delta_I + \delta_I^2) \text{ and } 1/T_2^{\beta} = 4J(0)(p^2 + 2\,C_{kl}\,p\,\delta_I + \delta_I^2)$$

respectively. $p = \mu_0/(8\pi\sqrt{2})\hbar\gamma_I\gamma_S/r_{IS}^3$, $\delta_I = 1/(3\sqrt{2})\gamma_I\Delta\sigma_I B_0$, μ_0 is magnetic permeability of vacuum, γ_I and γ_S are the gyromagnetic ratios of *I* and *S*, $\hbar$ is the Planck's constant divided by 2π, r_{IS} is the distance between *S* and *I*, B_0 is the polarizing magnetic field, $\Delta\sigma_I$ is the difference between the axial and the perpendicular principal components of the axially symmetric chemical shift tensors of spin *I*, $C_{kl} = 0.5(3\cos^2\Theta_{kl} - 1)$, and Θ_{kl} is the angle between the unique tensor axes of the interactions *k* and *l*.[7,13] Assuming in addition that the applied I^{β}-selective inversion pulse does not perturb I^{α}-magnetization, the SPI polarization transfer function can be expressed as

$$f_{SPI}(I_z \rightarrow 2I_zS_z) = \exp(-\tau\Delta\Omega/(T_2^{\beta}\Delta\Omega)) \qquad (1)$$

where an empirical expression for the inversion of a single line characterized by the given T_2 and infinitely long T_1 relaxation times suggested in refs 47−48 is used. In eq 1, $\Delta\Omega$ represents the bandwidth of a selective pulse defined as the width of the inversion profile at 3 dB less than the maximum amplitude (71%), and $\tau\Delta\Omega$ is an empirical parameter that is characteristic of the pulse-shape used. Thus, the most effective pulse should feature the smallest possible $\tau\Delta\Omega$ value while possessing a reasonably large bandwidth subject to the requirement that it does not significantly perturb the α-transition.

(21) Sorensen, O. W. *Prog. Nucl. Magn. Reson. Spectrosc.* **1989**, *21*, 503−569.
(22) Morris, G. A.; Freeman, R. *J. Am. Chem. Soc.* **1979**, *101*, 760−762.
(23) Ernst, R. R.; Bodenhausen, G.; Wokaun, A. *The Principles of Nuclear Magnetic Resonance in One and Two Dimensions*; Clarendon Press: Oxford, 1987.
(24) Bruschweiler, R. *Prog. Nucl. Magn. Reson. Spectrosc.* **1998**, *32*, 1−19.
(25) Bruschweiler, R. *Chem. Phys. Lett.* **1996**, *257*, 119−122.
(26) Riek, R.; Wider, G.; Pervushin, K.; Wuthrich, K. *Proc. Natl. Acad. Sci. U.S.A.* **1999**, *96*, 4918−4923.
(27) Khaneja, N.; Luy, B.; Glaser, S. J. *Proc. Natl. Acad. Sci. U.S.A.* **2003**, *100*, 13162−13166.
(28) Pachler, K. G. R.; Wessels, P. L. *J. Magn. Reson.* **1973**, *12*, 337−339.
(29) Chalmers, A. A.; Pachler, K. G. R.; Wessels, P. L. *Org. Magn. Reson.* **1974**, *6*, 445−447.
(30) Pachler, K. G. R.; Wessels, P. L. *J. Chem. Soc., Chem. Commun.* **1974**, 1038−1039.
(31) Dekker, T. G.; Pachler, K. G. R.; Wessels, P. L. *Org. Magn. Reson.* **1976**, *8*, 530−531.
(32) Pachler, K. G. R.; Wessels, P. L. *J. Magn. Reson.* **1977**, *28*, 53−61.
(33) Pachler, K. G. R.; Wessels, P. L. *Org. Magn. Reson.* **1977**, *9*, 557−558.
(34) Pachler, K. G. R.; Wessels, P. L. *Org. Magn. Reson.* **1980**, *13*, 100−104.
(35) Jakobsen, H. J.; Linde, S. A.; Sorensen, S. *J. Magn. Reson.* **1974**, *15*, 385−388.
(36) Sorensen, S.; Hansen, R. S.; Jakobsen, H. J. *J. Magn. Reson.* **1974**, *14*, 243−245.
(37) Vold, R. R.; Vold, R. L. *Prog. Nucl. Magn. Reson. Spectrosc.* **1978**, *12*, 79−133.
(38) Freeman, R.; Wittekoe. S.; Ernst, R. R. *J. Chem. Phys.* **1970**, *52*, 1529−1532.
(39) Khaneja, N.; Reiss, T.; Luy, B.; Glaser, S. J. *J. Magn. Reson.* **2003**, *162*, 311−319.
(40) Freeman, R.; Kupce, E. *J. Biomol. NMR* **2003**, *27*, 101−113.
(41) Kupce, E.; Nishida, T.; Freeman, R. *Prog. Nucl. Magn. Reson. Spectrosc.* **2003**, *42*, 95−122.
(42) Kupce, E.; Freeman, R. *J. Magn. Reson.* **2003**, *163*, 56−63.
(43) Kupce, E.; Freeman, R. *J. Magn. Reson.* **2003**, *162*, 300−310.
(44) Kupce, E.; Freeman, R. *J. Magn. Reson.* **2003**, *162*, 158−165.
(45) Skinner, T. E.; Reiss, T. O.; Luy, B.; Khaneja, N.; Glaser, S. J. *J. Magn. Reson.* **2003**, *163*, 8−15.
(46) Reiss, T. O.; Khaneja, N.; Glaser, S. J. *J. Magn. Reson.* **2003**, *165*, 95−101.
(47) Hajduk, P. J.; Horita, D. A.; Lerner, L. E. *J. Magn. Reson., Ser. A* **1993**, *103*, 40−52.
(48) Horita, D. A.; Hajduk, P. J.; Lerner, L. E. *J. Magn. Reson., Ser. A* **1993**, *103*, 53−60.

For the purpose of comparison, it is instructive to provide the corresponding function for the transfer efficiency of INEPT:

$$f_{\mathrm{INEPT}}(I_z \rightarrow 2I_zS_z) = \sin(\pi J_{IS}t_{\max})\exp(-t_{\max}/T_2) \qquad (2)$$

where $1/T_2 = {}^1/_2(1/T_2^{\alpha} + 1/T_2^{\beta})$ and $t_{\max} = 1/\pi J_{IS}\ \arctan(1/(\pi J_{IS}T_2))$. Providing that T_2 is not too much shorter than $1/J_{IS}$, eq 2 can be approximated by $f_{\mathrm{INEPT}}(I_z \rightarrow 2I_zS_z) = \exp(-1/(2J_{IS}T_2))$ which, in this form, can be directly compared with eq 1.

Equation 1 illustrates the effects of relaxation on the efficiency of SPI in a two-spin system. A more detailed treatment requires a numerical integration of the spin dynamics equation for the density operator in the presence of relaxation. This can be most conveniently done using the web-accessible program QSim (http://www.bpc.lu.se/QSim).[57] The simulations were performed for a three-spin $^1/_2$ system comprising a $^1H^N-^{15}N$ pair, coupled with $^1J_{HN} = 90$ Hz, and a third 1H spin at distances of 3.50 and 4.52 A from $^1H^N$ and ^{15}N, respectively, coupled with $^1J_{HH} = 10$ Hz to emulate the effect of the remote protons (at an 80% level of deuteration). Axially symmetric chemical shift anisotropy (CSA) tensors with $\Delta\sigma_N = -160$ ppm and $\Delta\sigma_H = -14$ ppm were used. The intramolecular dynamics are described by the model-free parameters typical of well-structured parts of a protein ($S^2 = 0.85$, $\tau_e = 50$ ps). The same rotational correlation times were kept for the auto- and cross-relaxation terms. The amide proton frequency was kept on resonance, while the offset of the remote proton frequency was set to 10^4 Hz to avoid perturbation of the remote proton. The simulations were performed at an external field strength $B_0 = 21.16$ T (900 MHz for protons). The RF field was 5 kHz for the hard pulses and as required for the selective pulses.

Hajduk et al.[47] estimated the $\tau\Delta\Omega$ parameter in eq 1 required for the inversion Gaussian pulse, applied on resonance, as 0.17 for the range of values $(T_2\Delta\Omega)^{-1} < 1$. Extending simulations into the range of shorter T_2's and off-resonance inversion using the program QSim shows that for $(T_2\Delta\Omega)^{-1} > 1$ the inversion efficiency deviates from the simple empirical form of eq 1. Thus, for $(T_2\Delta\Omega)^{-1}$ of 2.6, 5.2, and 10.4, the best fit of the inversion amplitude versus T_2 using the function described by eq 1 results in $\tau\Delta\Omega$ of 0.14, 0.12, and 0.09, respectively. The corresponding simulations with rectangular pulses $(T_2\Delta\Omega)^{-1}$ of 4.2, 8.5, and 17 delivered $\tau\Delta\Omega$ of 0.13, 0.10, and 0.08, respectively. Thus, for the purpose of qualitative comparison of PC−SPI with INEPT and CRIPT as applied to large proteins with rotational correlation time in the range of 100−200 ns, $\tau\Delta\Omega = 0.12$ and 0.10 were selected for PC−SPI using Gaussian and rectangular elementary pulses, respectively.

Complex Preparation. A fragment of CR1 corresponding to its complement control protein (CCP) modules 15, 16, and 17, which together constitute the functional site 2 of CR1, was expressed in *Pichia pastoris* and purified as described previously.[49] C3 was purified from human serum as described before.[50] An additional purification step consisting of a Mono S column (Pharmacia, Piscataway, NJ) with phosphate buffer at pH 6.0 was used. The pH of C3-containing fractions was raised to 7.5 and typsin-TPCK (Sigma, St. Louis, MO) was added. After incubating for 2 min at 37 °C the sample was concentrated and passed over a Superose-12 gel filtration column (Pharmacia). The purity of the C3b was greater than 95% as assessed by sodium dodecyl sulfate-polyacrylamide gel electrophoresis. The complex was prepared in 50 mM K phosphate buffer, pH 6, with 150 mM NaCl. A 0.05 mM solution of C3b was added to a 0.05 mM solution of CR1 and the mixture was then concentrated to give a final concentration of 0.4 mM complex. The assignments for the backbone ^{15}N and $^1H^N$ resonances of CR1 site 2 were obtained from previous work by Smith et al.[51]

Spectra Acquisition and Processing. All $^{15}N-^1H$ correlation spectra of the CR1/C3b complex were acquired at 37 °C on a Bruker spectrometer operating at 21.16 T equipped with a TXI probe. Total of 1024×64 or 1024×32 complex points were acquired in the directly and indirectly detected dimensions, respectively. For PC−SPI, a Gaussian frequency-modulated shaped pulse with an inversion profile characterized by bands with width of $\Delta\Omega = 30$ Hz offset by 180 Hz, or a rectangular frequency-modulated shaped pulse with bands characterized by $\Delta\Omega = 42$, was used. The offset of the PC−SPI pulse, at the low-frequency edge of the inversion profile, was set to 6 ppm in the first spectrum and increased by $2J_{NH}/8$ Hz for each consecutive spectrum. For comparison, a CRINEPT−HMQC TROSY[19] spectrum was acquired over 24 h. The spectra were processed using a Lorentzian-to-Gaussian window function with a 20 Hz line broadening factor in the ^1H dimension and an 80 Hz line broadening factor in the ^{15}N dimension; narrowing factors were 0.8 for ^1H and 1.0 for ^{15}N dimension in CRINEPT−HMQC TROSY and 1.0 in both dimensions for PC−SPI TROSY spectra.

Results and Discussion

Broadband SPI Using Polychromatic Pulse. Broadband SPI is implemented by using a polychromatic pulse, which is generated by a group of N essentially simultaneous elementary soft pulses of different frequencies.[52,53] To achieve this, the shape of an elementary soft pulse is repeatedly multiplied with a sinusoidal function until the required number of inversion bands is obtained, as described in ref 54. The elementary soft pulse can be selected for use in PC−SPI on the basis of minimal $\tau\Delta\Omega$, suggesting either a constant-amplitude (rectangular) or a Gaussian pulse truncated at 5% of its maximum amplitude[47] as a building block for this technique. When applied to the $^1H^N-^{15}N$ spin system with $J_{NH} = 90$ Hz, the frequency separation between adjacent inversion maxima should be 180 Hz or $2J_{IS}$, with a corresponding number of pulses (N) of approximately 20 to cover the entire $^1H^N$ region of a typical protein. The most efficient inversion profile for this technique is characterized by the largest possible "filling factor" $\Delta\Omega$, that is, the most complete inversion, with the width of an individual inversion maximum approaching J. The duration of the elementary pulse and the level of truncation should be adjusted to ensure the best performance of the PC−SPI pulse. For example, $\Delta\Omega$ is inversely proportional to the pulse duration, favoring shorter pulses. On the other hand, a pulse that is too short produces interference between inversion bands, which results in deterioration of the desired excitation profile and spin trajectories[54] although to some extent this can be reduced by Bloch−Siegert compensation.[55] An advantage of the polychromatic inversion is the fact that near-optimal trajectories of the individual components of the spin magnetization can be achieved even in situations where the width of the individual inversion bands is comparable to the frequency separation between bands. This effect can be attributed to the constructive interference between individual inversion pulses closely spaced in the frequency domain.

(49) Kirkitadze, M. D.; Krych, M.; Uhrin, D.; Dryden, D. T. F.; Smith, B. O.; Cooper, A.; Wang, X. F.; Hauhart, R.; Atkinson, J. P.; Barlow, P. N. *Biochemistry* **1999**, *38*, 7019−7031.
(50) Nickells, M. W.; Atkinson, J. P. *J. Immunol.* **1990**, *144*, 4262−4268.
(51) Smith, B. O.; Mallin, R. L.; Krych-Goldberg, M.; Wang, X. F.; Hauhart, R. E.; Bromek, K.; Uhrin, D.; Atkinson, J. P.; Barlow, P. N. *Cell* **2002**, *108*, 769−780.
(52) Kupce, E.; Freeman, R. *J. Magn. Reson., Ser. A* **1993**, *105*, 234−238.
(53) Kupce, E.; Freeman, R. *J. Magn. Reson., Ser. A* **1993**, *102*, 122−126.
(54) Freeman, R. *Prog. Nucl. Magn. Reson. Spectrosc.* **1998**, *32*, 59−106.
(55) Steffen, M.; Vandersypen, L. M. K.; Chuang, I. L. *J. Magn. Reson.* **2000**, *146*, 369−374.

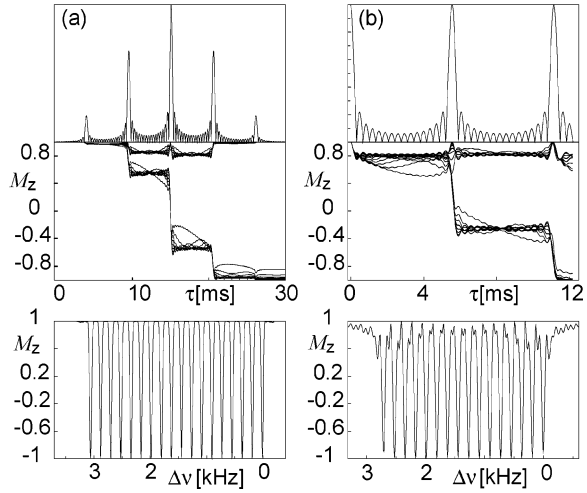

Figure 1. Shape (top), time evolution of magnetization vectors with the frequency offsets of 90**i* Hz, *i* = 0, 1, ...36 (middle), and excitation profile (bottom) of PC−SPI in the absence of relaxation generated using (a) a 30-ms Gaussian inversion pulse and (b) a 20-ms rectangular pulse truncated at 12.16 ms and $\gamma B_2 = 520$ Hz.

Figure 1a shows the shape and time evolution of magnetization vectors with frequency offsets of 90**i* Hz, *i* = 0, 1, ...36, and the calculated excitation profile of PC−SPI generated using a 30-ms Gaussian inversion pulse with $\Delta\Omega = 33$ Hz in the absence of relaxation. The inversion of magnetization shows clearly defined steps and is almost complete after 20 ms. Therefore, for practical applications, it is reasonable to truncate the pulse at this time point. A still larger $\Delta\Omega = 42$ Hz and more sinusoidal excitation profile can be obtained by employing a 20-ms rectangular pulse truncated at 12.16 ms, achieving 90% of inversion (Figure 1b). A comparison of Figure 1a and b shows that it is probably feasible to obtain a still shorter pulse by employing direct optimization.[56] One such attempt is presented in Supporting Information.

Comparison of Transfer Efficiencies. The calculated efficiency of the polarization transfer for Gaussian and rectangular pulse-based PC−SPI was compared to the efficiency of INEPT transfer, as a function of rotational correlation time. An isolated $^1H-^{15}N$ moiety with $r_{HN} = 1.02$ A, $\Delta\sigma_N = 160$ ppm, and $\Delta\sigma_H = 14$ ppm, and with intramolecular dynamics described by model-free parameters typical of a well-structured region of a protein ($S^2 = 0.85$, $\tau_e = 50$ ps), was used. While the efficiency of the polarization transfer using SPI is comparable to that of INEPT when acting on the fast relaxing component of the ^1H multiplet (anti-TROSY), the inversion of the slowly relaxing (TROSY) component results in a moderate drop in the efficiency of polarization transfer by SPI and this is particularly conspicuous for very large molecules. Overall, the gain in sensitivity (efficiency of the polarization transfer) of SPI versus INEPT stems from the more favorable relaxation properties of the density operator along the SPI trajectory compared to that of INEPT.[27] The trajectories of the density operator in the two-spin system realized by the PC−SPI pulse, and by an optimal pulse called CROP,[27] are very similar. This results in a similar transfer efficiency calculated for the optimal trajectory using eq 1 and eqs 5 and 6 in ref 27, respectively. Indeed, for a $^1H-^{15}N$ spin system (see Methods) and $B_0 = 21.16$ T, the ratio of the cross-correlated to the auto-correlated relaxation rates, k_c/k_a, was calculated to be 0.94. For a hypothetical molecule with $\pi k_a/J = 2.44$, the maximal theoretical transfer efficiency is $\eta = 0.81$. Our numerical simulations using the program QSim (for a two-spin system using a 30-ms Gaussian inversion pulse truncated at 22.3 ms) result in $\eta = 0.75$. A quantitative experimental comparison of polarization transfer efficiencies between SPI pulses and CROP sequences requires fine-tuning of many parameters such as, for example, truncation levels of the pulses as well as knowledge of the experimental values of k_a and k_c, essential for calculating relaxation rate-dependent CROP rf-shapes. Therefore, this calls for separate experimental and theoretical studies, which will be reported elsewhere. Even in the absence of interference effects ($T_2^\alpha = T_2^\beta = T_2$), the predicted decay of the polarization transfer efficiency as a function of T_2 is more than twice as slow in SPI as it is in INEPT; for example, compare $f_{SPI} = \exp(-1/(420\ T_2))$ and $f_{INEPT} = \exp(-1/(180\ T_2))$, when $J_{IS} = 90$ Hz, $\Delta\Omega = 42$ Hz, and $\tau\Delta\Omega = 0.1$ are used in eqs 1 and 2.

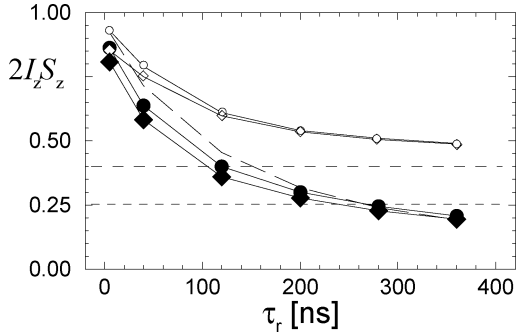

Figure 2. Simulations of the efficiency of polarization transfer $I_z \rightarrow 2I_zS_z$ in a three-spin system (see Methods) using the program QSim. CRIPT transfer efficiency is shown as two horizontal dashed lines for 500 (short dash) and 900 (dash) MHz. The long-dashed line indicates the efficiency of an INEPT transfer. Open and closed symbols indicate the polarization transfer efficiency for the cases where the TROSY and anti-TROSY components of the doublet, respectively, are inverted by PC−SPI. Circles indicate PC−SPI with the frequency-modulated Gaussian pulse and diamonds indicate PC−SPI with the frequency-modulated rectangular pulse.

A quantitative theoretical comparison of PC−SPI with INEPT and CRIPT was also performed in a three-spin system emulating the effect of relaxation due to the presence of remote protons. Figure 2 shows the calculated polarization transfer efficiencies for SPI, INEPT, and CRIPT (at 500 and 900 MHz for protons), which largely confirm conclusions made on the basis of eqs 1 and 2. At the small τ_r values (compare data for $\tau_r = 5$ ns in Figure 2), the efficiency of the magnetization transfer of the slow-relaxing component (TROSY) by PC−SPI is comparable to that of INEPT transfer providing that the inversion profile of the selective pulse is close to an ideal 100% inversion, as achieved with the Gaussian pulse. With the truncated rectangular pulse tested in the current work, the inversion is not fully achieved (see Figure 1) causing a loss in sensitivity at the lower correlation times. For rotational correlation times of 120 ns and higher, however, this effect becomes negligible as the shorter duration of the SPI benefits the transfer. The PC−SPI-based transfer has been demonstrated to have higher calculated efficiency than CRIPT at 900 MHz for correlation times of up to 360 ns.

Design of PC−SPI-Based 2D [$^1H^N$,^{15}N]-TROSY. Figure 3 shows an experimental scheme for the use of PC−SPI for the

(56) Kupce, E.; Freeman, R. *J. Magn. Reson., Ser. A* **1993**, *103*, 358−363.
(57) Helgstrand, M.; Allard, P. J. *Biomol. NMR* **2004**, *30*, 71−80.

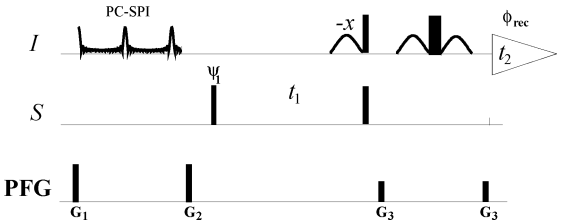

Figure 3. Experimental scheme of PC−SPI TROSY. The rows marked *I* and *S* represent the rf-channels irradiating the ^{1}H and ^{15}N spins, respectively. Narrow and wide bars stand for 90° and 180° pulses, respectively. Open shapes, except for the shape marked PC−SPI, are 90° water-selective pulses. All phases are set to {*x*}, unless indicated otherwise. The line marked PFG (pulsed field gradient) indicates the magnetic field gradients applied along the *z*-axis: G_1, amplitude = 80 G/cm, duration = 0.5 ms; G_2, 80 G/cm, 0.9 ms; G_3, 60 G/cm, 0.5 ms. Phases are $\psi_1 = \{x, -x\}$, $\phi_{rec} = \{y, -y\}$. The phase-sensitivity in the ^{15}N (t_1) dimension is obtained by the States-TPPI method applied to ψ_1. The settings used for the PC−SPI pulse sequence are indicated in the text. For the purposes of comparison, the PC−SPI element was replaced with INEPT with the duration set to $1/2J_{IS}$.

construction of a 2D [$^1H^N$,^{15}N]-TROSY suitable for large proteins or protein complexes. A PC−SPI pulse is used to create two-spin order magnetization, which can be subsequently converted to an antiphase coherence by the use of a hard pulse on the ^{15}N channel followed by chemical shift evolution and conversion to ^{1}H antiphase magnetization. In this experiment, transverse relaxation optimization based on the constructive interference between dipole−dipole and CSA interactions is active throughout the entire experiment. All four components of the ^{15}N−^{1}H system are recorded without *J*-refocusing, which allows the pulse sequence to be kept short so as to further counteract the effects of relaxation.

A single application of the PC−SPI TROSY pulse sequence produces a coupled 2D [$^1H^N$,^{15}N]-correlation spectrum. The intensities of resonances in the directly detected dimension are modulated with a periodic function coinciding with the excitation profile of the PC−SPI pulse (see Figure 5 and Figure 2S and 3S in Supporting Information), giving signals with positive and negative amplitudes in adjacent bands. The negative bands can be inverted by multiplication with −1 after processing of the spectrum. To achieve this, a periodic step function with steps of amplitude 1 and −1 is created, the negative steps coinciding with the negative bands in an individual PC−SPI spectrum. The spectrum is then multiplied with this step function resulting in a corrected spectrum in which all nonfolded cross-peaks have positive intensities. To reconstruct a complete 2D spectrum in which resonances have nonartifactual intensities, the experiment must be repeated $n = 2-8$ times with the PC−SPI pulse shifted in the frequency domain in steps of $2J_{IS}/n$. Assuming that the modulation profile has a sinusoidal shape averaged over the entire bandwidth of PC−SPI, the fraction of the starting in-phase magnetization transferred to the two-spin order is $2/\pi$ [i.e., the ratio of the integral from 0 to *J* of a sine function with period 2*J* to the integral of a value 1 constant function (absolute transfer), over the same range]. This value is approached for SPI with optimized $\Delta\Omega$. This type of spectral reconstruction results in in-phase appearance of 2D multiplets in both spectral dimensions (see Figure 5a).

PC−SPI Applied to 200 kDa CR1/C3b Complex. Slices taken from the individual PC−SPI spectra acquired with the Gaussian profile as discussed above (Figure 5b and c) can be compared with the reconstructed spectrum (Figure 5a) and the CRINEPT−HMQC−TROSY spectrum (Figure 5d). Each PC−

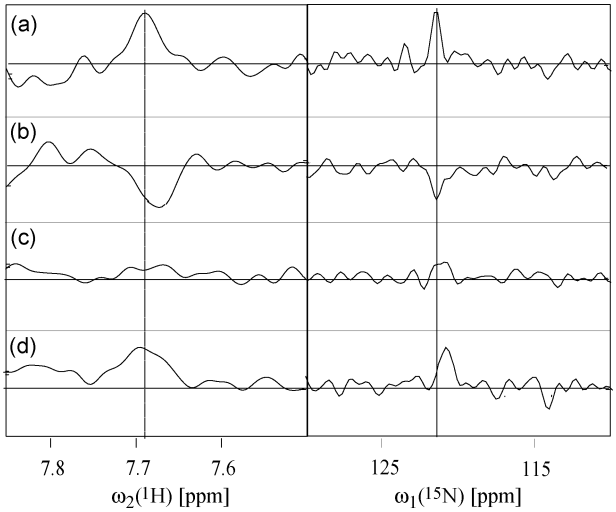

Figure 4. 1D slices along the ^{1}H and ^{15}N dimensions of 2D [^{1}H,^{15}N]-correlation spectra of the CR1/C3b complex (see Methods). In a and b, the spectra are measured with the experimental scheme of Figure 3 using the PC−SPI pulse of Figure 1b. The slices in a and b correspond to the selective inversion of the TROSY and anti-TROSY ^{1}H mutliplet components, respectively. In c, the corresponding slices are taken from the INEPT-based polarization transfer directly substituting PC−SPI in Figure 3. In d, the slice is taken from the 2D CRINEPT−HMQC experiment.[26] For all spectra, acquisition parameters are set up identically. Sixty-four scans per t_1 increment and 120 increments with 0.5-s interscan delay were collected resulting in the aquisition time per PC−SPI and INEPT based experiments of 1.3 h. The CRINEPT−HMQC spectrum was measured in 3 h using 148 scans per t_1 increment. The vertical dashed line indicates ^{1}H chemical shift of E1042.

SPI spectrum was acquired over 7 h. The signals inverted on-resonance have an intensity 2.4 times that of the CRINEPT spectrum, with an equal length of acquisition. To acquire and reconstruct a complete 2D spectrum (Figure 5a), with nonartifactual signal intensities, eight such spectra were needed. A further comparison with CRINEPT−HMQC−TROSY and INEPT of the individual PC−SPI spectra acquired using the rectangular pulse of Figure 1b, and processed in the manner described above, is shown in Figure 3S in Supporting Information. Further optimization of the PC−SPI shape to reach a higher "filling factor", that is, $\Delta\Omega$, would allow reconstruction of a complete correlation map with fewer elementary PC−SPI spectra. To maintain the TROSY effect in the indirectly detected dimension, no refocusing 180° ^{1}H pulse was applied during the t_1 evolution resulting in a coupled ^{1}H−^{15}N correlation spectrum. No special efforts were made to suppress unwanted multiplet components, which on average correspond to 10−30% of the strongest TROSY component. Because of the distinct antiphase pattern of the doublets in the directly acquired dimension, the presence of these residuals did not represent a significant problem during interpretation of spectra.

This qualitative difference in the relaxation behavior of SPI and INEPT is confirmed by this experiment. Figure 4a and 4b provides a comparison of intensities of the CR1 residue E1042 cross-peak in the 200 kDa complex with C3b for the situations where either the TROSY or the anti-TROSY component of the ^{1}H multiplet is actively inverted. The CRINEPT-based polarization transfer delivers a comparable signal intensity to that measured with PC−SPI, as is predicted by calculations. For this complex, the INEPT-based transfer is the least efficient as can be seen in the 1D slices shown in Figure 4. The main advantage of PC−SPI is that it does not rely on the significant

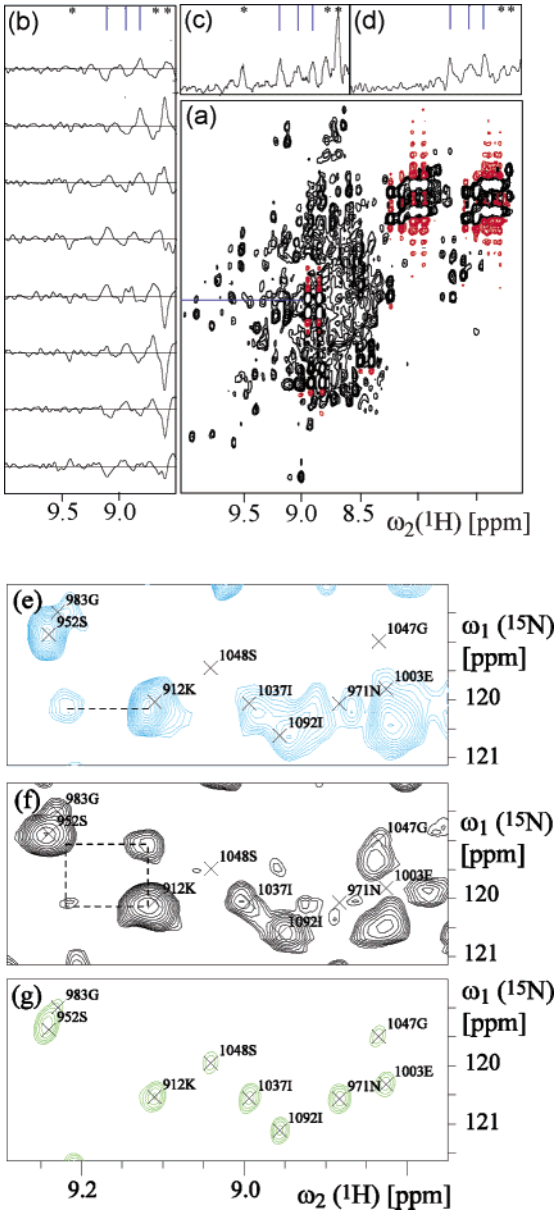

Figure 5. PC−SPI spectra of the CR1(site 2)/C3b complex. Panel a shows the reconstructed 2D PC−SPI spectrum. The horizontal line at 121.5 ppm indicates the position of the strips presented in panels b and c. Panel b shows the strips taken through the individual PC−SPI spectra. Each PC−SPI spectrum was acquired in 7 h with 312 scans per one t_1 increment and 128 increments with 0.5-s interscan delay. Vertical lines indicate I1037, N971, and an unidentified resonance. Stars indicate examples of overlap that arise from the anti-TROSY components of the strong resonances at higher ppm. The equivalent strip taken from a CRINEPT−HMQC spectrum is shown in panel d. In e and g, fragments of 2D CRINEPT−HMQC and PC−SPI spectra measured with the CR1(site 2)/C3b complex are shown. A dashed line in e and dashed rectangle in g outline the observed 2D multiplet patterns. To illustrate chemical shift perturbation induced by complexation, the corresponding fragment of the 2D TROSY spectrum measured with CR1(site 2) alone is shown in g and the spectrum in e is shifted by 45 Hz.

difference in transverse relaxation of the two multiplet components called TROSY and anti-TROSY, thus resulting in more uniform cross-peak intensities as well as less stringent demands on the strength of the polarizing magnetic field. Another crucial advantage of the PC−SPI based experiments over CRINEPT HMQC is the fact that the PC−SPI scheme produces the anti-phase $^{15}N-^{1}H$ coherence which is used for the detection of ^{15}N

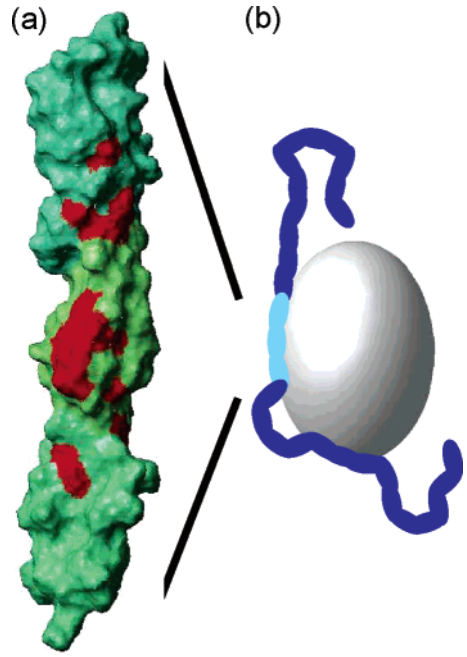

Figure 6. Characterization of the CR1−C3b interaction by PC−SPI. In panel a, those CR1 amino acid residues whose NH resonances are either shifted or differentially broadened to a significant extent upon complex formation are marked in red on the surface of the structure of CR1(site 2). The three modules which constitute site 2 are distinguished by different shades of green, with the 15th module shown at the top and the 17th at the bottom. (b) A cartoon showing the position of site 2 (pale blue) within CR1 (dark blue) and the interaction with C3b (gray). To simplify the graphics, the attachment of CR1 to the erythrocyte is not shown.

chemical shifts generating significantly narrower lines along ^{15}N dimension because of the TROSY effect as it can be seen in Figure 4a and d, respectively. This is translated to significantly better resolved 2D correlation spectra obtained using PC−SPI comparing to CRINEPT−HMQC shown in Figure 5b. For example, the absence of the cross-peak stemming from the amino acid 1003E is clearly confirmed in the PC−SPI spectrum (Figure 5f) while the analysis of chemical shift perturbations is hampered by lower spectral resolution in the CRINEPT−HMQC spectrum (Figure 5e).

Because of in-phase appearance of 2D multiplet structures of cross-peaks in PC−SPI spectra, no spectral intensity is lost in situations when TROSY and anti-TROSY components stemming from different cross-peaks overlap in the crowded regions of spectra. In our experience, the correct recognition of 2D multiplet components in PC−SPI spectra, which is essential for interpretation of spectral information, can be facilitated by simultaneous inspection of the corresponding regions in the CRINEPT−HMQC spectra as it is illustrated in Figure 5e and f. Thus, it is instructive to complement the PC−SPI experiment with the CRINEPT−HMQC-type of experiments to maximize the amount of interpretable spectral information for critical biological applications.

The PC−SPI spectra acquired with the CR1 (site 2)/C3b complex sample allowed the identification of 28 backbone NH signals in CR1 that undergo significant chemical shift perturbations, or differential broadening, upon forming the complex with C3b. The corresponding residues are shown on the surface representation of CR1 (site 2) (Figure 6) and may represent contact sites on CR1 for C3b. Of interest are not only those residues whose side chains form a surface patch toward the

middle of the central module, but also those residues near intermodular interfaces; perturbations of chemical shifts in these regions indicate the possibility of intermodular rearrangement upon formation of the complex.

Conclusions

We have proposed a method for the broadband extension of the polarization transfer on the basis of selective inversion of spin populations using multiband (polychromatic) irradiation. An interesting advantage of the polychromatic inversion is the fact that near-optimal trajectories of the individual components of the spin magnetization can be achieved even in situations where the width of the individual inversion bands is comparable to the frequency separation between bands. This effect can be attributed to the constructive interference between individual inversion pulses closely spaced in the frequency domain. We have tested our approach with a large protein complex (∼200 kDa) and demonstrated significant improvements over conventional techniques.

Acknowledgment. Financial support was obtained from Swiss National Science Foundation grant to K.P.; the Edinburgh group is supported by MRC (U.K.), K.B. is an MRC Postdoctoral Training Fellow.

Supporting Information Available: Figure 1S showing the characteristics of the truncated rectangular pulse; Figure 2S showing polarization transfer as a function of offset frequency calculated for an isolated two-spin system; and Figure 3S showing strips taken from PC−SPI spectra acquired using the pulse defined in Figures 1b and 1S, compared to that acquired using INEPT transfer. This material is available free of charge via the Internet at http://pubs.acs.org.

JA0462326